Optics Letters

Control the Raman response of individual carbon nanotubes by orbital angular momentum of light

Fajun Xiao,[1,6] Can Liu,[2] Kaihui Liu,[2,4] Wuyun Shang,[1] Weiren Zhu,[3] and Jianlin Zhao[1,5]

[1]MOE Key Laboratory of Material Physics and Chemistry under Extraordinary Conditions, and Shaanxi Key Laboratory of Optical Information Technology, School of Science, Northwestern Polytechnical University, Xi'an 710129, China
[2]State Key Laboratory for Mesoscopic Physics, School of Physics, Peking University, Beijing 100871, China
[3]Department of Electronic Engineering, Shanghai Jiao Tong University, Shanghai 200240, China
[4]e-mail: khliu@pku.edu.cn
[5]e-mail: jlzhao@nwpu.edu.cn
[6]e-mail: fjxiao@nwpu.edu.cn

Received 27 April 2017; revised 26 May 2017; accepted 30 May 2017; posted 1 June 2017 (Doc. ID 294638); published 22 June 2017

We propose and demonstrate an approach for tailoring the Raman response of an individual single-walled carbon nanotube (SWNT) by employing the optical vortex as the excitation. Specifically, we observe the blueshifts of radial breathing mode and *G* mode when the topological charge of the vortex beam is increased from 0 to 5. Further theoretical analysis yields that the optical absorption and the corresponding laser heating effect of SWNT are inversely proportional to the topological charge of the optical vortex. Such a decrease in the laser heating effect weakens the softening of C–C bonds, leading to the blueshifts of Raman modes.

OCIS codes: (050.4865) Optical vortices; (300.6450) Spectroscopy, Raman; (160.4236) Nanomaterials.

https://doi.org/10.1364/OL.42.002491

A single-walled carbon nanotube (SWNT), a one-dimensional (1D) tubular form of graphitic structure, has attracted tremendous interest owing to its outstanding electrical and optical properties. Tailoring the properties of an SWNT is of central importance for the low-dimensional physics and the next-generation nanoelectronic and nanophotonic devices [1–3]. In the field of optics, the SWNT can be treated as an optical nanoantenna [4], which can interplay with the vicinity photonic nanostructures including plasmonic structures [5–8] and photonic microcavities [3,9] via near-field coupling. Recent studies have revealed that integrating photonic nanostructures with SWNTs is capable of engineering photophysical properties of SWNTs, leading to not only the fundamental interesting phenomena such as selection rule breakdown [7], localization of excitons [10], and exciton-plasmon nonlinearity [5], but also the promising applications in light harvesting [6] and nanoscale lasers [11]. An alternative yet more flexible way to tune photophysical properties of the optical antenna is employing the phase structure of the illumination field. It has been demonstrated that a light field with a temporal- or spatial-shaped phase structure can coherently control the plasmon resonance of optical nanoantennas [12–14]. Such an unconventional approach breaks the limit of the nanostructure geometry, enabling the desirable near-field distribution [14] and far-field scattering spectrum [12].

An optical vortex, as a renowned phase-structured light, possesses a helical phase front, which varies continuously along the azimuthal direction by $2l\pi$ ($l = \pm 1, 2, \ldots$). As a result, the optical vortex carries an intrinsic orbital angular momentum (OAM) content denoted as $l\hbar$ per photon that is expected to add more freedom for actively controlling the light matter interaction at nanoscale [15,16]. However, to date the importance of the OAM to the photophysical properties of the ideal 1D optical nanoantenna, i.e., carbon nanotube, has not yet to be elucidated. Here, we report that the optical vortex can manipulate the Raman response of an individual SWNT due to its ability to control the optical absorption of the materials. Remarkably, when the topological charge of the optical vortex is increased from $l = 0$ to $l = 5$, the SWNTs show obvious blueshifts in Raman modes. Our study shows a flexible way to control the photophysical properties of the SWNT and provides an understanding of the OAM-involved light matter interaction in single molecular level.

The substrate used in this study is a Si_3N_4/Si wafer with an open slit of ~40 μm width and 0.6 mm length. The open slit was fabricated on the substrate using standard photolithography and wet etching processes [17]. The isolated SWNTs were grown across the slit by the chemical vapor deposition (CVD) method using methane in hydrogen (CH_4:H_2 = 1:2) as feedstock and an ultrathin film (~0.25 nm) of Fe as the catalyst [18,19]. The atomic structures of SWNTs were determined from the electron-diffraction measurements using nanofocused 80 keV electron beams in a JEOL 2100 transmission electron microscope (TEM) [20]. Taking the slit edges as landmarks, the same SWNT can be identified in both TEM and microRaman setups.

In the optical measurement, the optical vortices were generated by employing the digital holography technique. The optical vortex can be written in polar coordinates (r, ϕ) as

$$E(r,\phi) = \mathrm{Ar}^{|l|}e^{-r^2/w_0^2}e^{il\phi}, \quad (1)$$

where A, l, and w_0 are the electric field amplitude, OAM content-related topological charge, and beam waist, respectively. The interference between the optical vortex and a plane wave forms a fork-like hologram, which is displayed onto a spatial light modulator (SLM). The optical vortex is reconstructed by directing a reference beam onto the SLM [21] and is then used as the excitation beam in the microRaman setup. In the Raman measurements, the excitation beam with wavelength of 532 nm was focused on the individual SWNTs with a spot size of ~1 μm^2 by an objective (50 ×, N.A. 0.55) [22]. The Raman spectra of SWNTs were measured at room temperature and ambient pressure, using a spectrometer (SR303i, Andor).

Figure 1 displays the electron diffraction pattern (EDS) and the Raman spectra of an individual SWNT. The EDS [Fig. 1(a)] allows us to determine the chiral indices of the SWNT to be (31,0), implying that this SWNT is a zigzag nanotube with a diameter of 2.43 nm. The SWNT (31,0) shows a strong resonant Raman spectrum of radial breathing mode (RBM) locating at 94 cm^{-1} as shown in Fig. 1(b). The Raman spectra covering D band and G band photons are also displayed in Fig. 1(b), suggesting the absence of D mode Raman peak and the G mode frequency of 1594 cm^{-1}. This means our suspended SWNT is of high quality with very low density of defects and without the uniaxial strain [23]. We also examine the polarization properties of RBM and G mode shown in Figs. 1(c) and 1(d), respectively. It is suggested that the Raman signals of both RBM and G mode are maximum with the incident polarization parallel to the tube and minimum when perpendicular, exhibiting a $\cos^2\theta$ pattern as the polarization angle θ varying. This observed depolarization effect reflects the antenna nature of 1D SWNTs [24].

In the following, we keep the power of the Raman excitation beam as a constant of 1 mW and investigate the Raman response of the SWNT (31,0) under the excitations of optical vortices with different topological charges. Figures 2(a)–2(f) depict the intensity distributions of a Gaussian beam ($l = 0$) and optical vortices with different topological charges, respectively. The topological charges (or the phase profiles) of these optical vortices are confirmed by the interferograms between the vortex beams and an inclined plane wave as shown in the insets of Figs. 2(b)–2(f). The fork-like fringes indicate the topological charges in Figs. 2(b)–2(f) range from $l = 1$ to $l = 5$, respectively. Figure 2(g) presents the Raman spectra of the SWNT (31,0) under the excitations as shown in Figs. 2(a)–2(f). An interesting feature emerges such that the increase of the topological charge (OAM content) of Raman excitations leads to an increase in the frequency for both RBM and G mode.

It has been reported that the carbon nanotube can be heated by the laser illumination [25–27]. Especially for the suspended carbon nanotube, the heat cannot be efficiently conducted away from the nanotube. Therefore, a considerable temperature rise in nanotube can be observed when the laser power increases. As the consequence of the temperature rise, the softening of C–C bonds occurs [28,29], leading to a redshift of Raman modes. Owing to the laser heating effect being proportional to the optical absorption, the blueshifts of RBM and G mode in Fig. 2(g) is ascribed to the OAM-mediated optical absorption decrease. To confirm the origin of the shifts of Raman modes, we then perform a full-wave simulation to extract the optical absorption of the SWNT (31,0). The absorption of SWNTs is closely related with their atomic and underlying electronic structures. According to the tight-binding theory and experiment results of Rayleigh scattering, the electron dispersion relation for zigzag nanotubes is given by [30–33]

$$E = E_c - E_v + \Delta E = 2\gamma_0\sqrt{1 + 4\cos\left(\frac{3bp_z}{2\hbar}\right)\cos\left(\frac{\pi s}{m}\right) + 4\cos^2\left(\frac{\pi s}{m}\right)} + \Delta E, \quad (2)$$

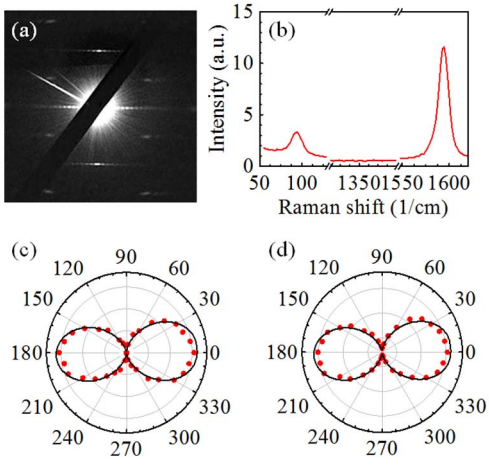

Fig. 1. Electron diffraction pattern (EDS) and Raman spectra of single-walled carbon nanotube (SWNT). (a) EDS of an individual SWNT allows us to determine its chiral indices as (31,0). (b) Raman spectrum of SWNT (31,0) under the excitation of a Gaussian beam. Peak intensities of the (c) RBM and (d) G mode as a function of polarization angle of the excitation. Here, the red dots and solid lines in (c) and (d) are experiment results and fittings results using $I(\theta) \propto \cos^2(\theta)$, respectively.

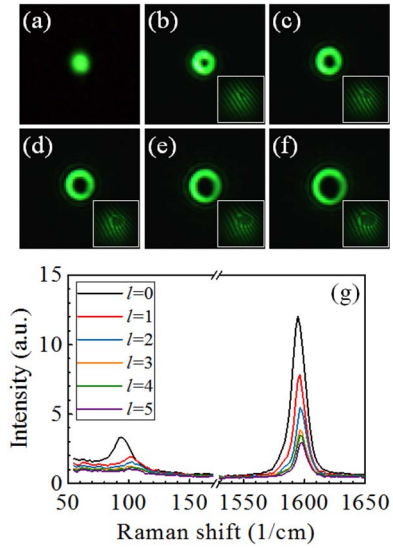

Fig. 2. Intensity distributions of the pump laser beams and their excited Raman spectra of SWNT (31,0). (a)–(f) Intensity distributions of Gaussian ($l = 0$) and optical vortices with topological charge from $l = 1$ to $l = 5$, respectively. The insets of (b)–(f) are the interference patterns between the Raman excitations with a plane wave. (g) Raman spectra of SWNT (31,0) under the excitation of Gaussian and optical vortices as shown in (a)–(f).

where p_z is the axial projection of the electron's quasi-momentum, s is the interband transition order, $E_{c(v)}$ is the conduction (valence) band energy, $\gamma_0 = 2.7$ eV is the overlap integral, $b = 0.142$ nm is interatomic distance, $\hbar$ is the reduced plank constant, m is the first chiral index, and ΔE accounts for the band gap energy contributed from many body and exciton effects. In our simulation, we set $\Delta E = 0.15$ meV according to the optical transition energy of SWNTs measured by the Rayleigh scattering [33]. Within the framework of quantum transport theory, the conductivity σ_{cn} is described as [34]

$$\sigma_{cn} = -\frac{ie^2\omega}{\pi^2\hbar r_c}\left\{\frac{1}{\omega(\omega + i/\tau)}\sum_{s=1}^{m}\int_{1stBZ}\frac{\partial F_c}{\partial p_z}\frac{\partial E_c}{\partial p_z}\mathrm{d}p_z - 2\sum_{s=1}^{m}\int_{1stBZ}E_c|R_{c,v}|^2\frac{F_c - F_v}{\hbar^2\omega(\omega + i/\tau) - 4E_c^2}\mathrm{d}p_z\right\}. \quad (3)$$

Here, e is electron charge, r_c is the radius of carbon nanotube, ω is the circular frequency of light, τ is the relaxation time, and $F_{c,v}$ is the equilibrium Fermi distribution function with the form of [34]

$$F_{c,v}(p_z, s) = \left\{1 + \exp\left[\frac{E_{c,v}(p_z, s) - \mu_{ch}}{k_B T}\right]\right\}^{-1}, \quad (4)$$

where $\mu_{ch} = 0$ is the chemical potential, k_B is the Boltzmann constant, T is the temperature, and $R_{c,v}$ is the normalized matrix elements of the dipole transition between conduction and valence bands. For a zigzag nanotube, we have [34]

$$R_{c,v}(p_z, s) = -\frac{b\gamma_0^2}{2E_c^2(p_z, s)}\left[1 + \cos\left(\frac{3b}{2\hbar}p_z\right)\cos\left(\frac{\pi s}{m}\right) - 2\cos^2\left(\frac{\pi s}{m}\right)\right]. \quad (5)$$

Then, the permittivity of the carbon nanotube is written as

$$\varepsilon = 1 - \frac{i\sigma_{cn}}{\varepsilon_0\omega}, \quad (6)$$

where ε_0 is vacuum permittivity.

The optical absorption of the SWNT (31,0) is numerically calculated by using the finite element method. In the simulation, we employ a perfectly matched layer as the boundary condition. The SWNT with the permittivity described by Eq. (6) is surrounded by air. The diameter and length of the nanotube are, respectively, set as 2.43 nm and 1.5 μm (larger than the beam diameter [1 μm] at the focus plane). The excitation beam defined by Eq. (1) has a wavelength of 532 nm, and the temperature is 300 K. The calculated absorption changes of SWNT (31,0) resulted from the OAM are shown in Figs. 3(a) and 3(b) (the red rectangles). It is clearly seen that absorption is gradually suppressed with the increasing of the topological charge of the Raman excitation. We ascribe such change in absorption as a consequence of the mismatching between the optical transition of the SWNT and the OAM of the excitation field. For SWNTs, the optical absorption is dominated by the dipole-allowed transitions between the Van Hove singularities. In the view of momentum conservation, the light field carrying the OAM excites the dipole transition inefficiently compared to the Gaussian beam [35]. Moreover, within the framework of the coherent interaction, the amount of overlapping between the optical vortex and the dipole-like eigenstate of the SWNT decreases as the OAM is increased [36]. Therefore, the transition rate or the absorption of the SWNT decreases with the increasing of topological charge, resulting in the blueshifts of

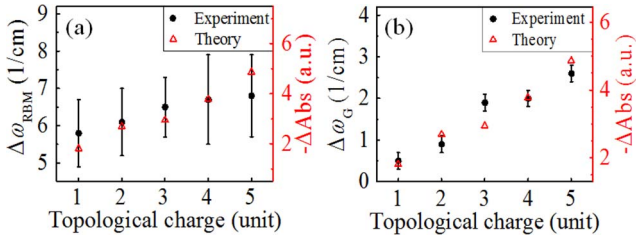

Fig. 3. Raman frequency shifts of (a) RBM and (b) G mode of SWNT (31,0) versus the topological charge of the optical vortex. The black dots and red triangles are the experiment and theory results, respectively.

Raman modes. We further obtain the frequencies of the Raman modes in Fig. 2(g) through a Lorentzian lineshape fitting. Qualitative comparisons between the shifts of Raman modes and the absorption change are displayed in Fig. 3, where the black dots in Figs. 3(a) and 3(b) are the frequency shifts of RBM mode and G mode, respectively. It suggests that the blueshifts of Raman modes and the absorption decrease almost obey the same trend, confirming that the blueshifts of Raman modes originate from the decrease of the optical absorption and the corresponding laser heating effect.

We also show the vortex excited Raman spectra of two chiral SWNTs in Fig. 4. The chiral indices of SWNTs in Figs. 4(1) and 4(2) are, respectively, determined to be (27,15) and (25,4) according to the EDS shown in Figs. 4(a1) and 4(a2). For both SWNTs, blueshifts of RBM and G mode are observed when the topological charge of the excitation is increased from 0 to 5, as shown in Fig. 4(b). More explicit Raman mode shifts of these two chiral SWNTs are illustrated in Figs. 4(c1) and 4(c2), exhibiting the same trend as those of the zigzag SWNT (31,0)

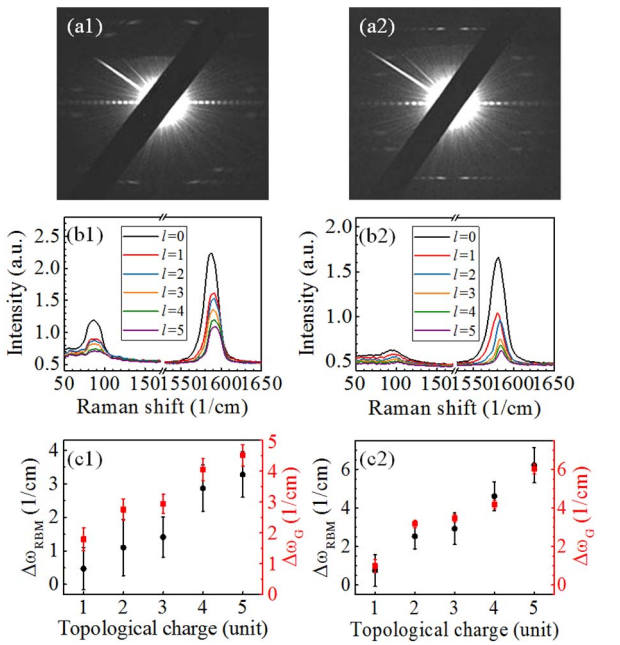

Fig. 4. Vortex-controlled Raman response of chiral SWNT (1) (27,15) and (2) (25,4). (a) EDS, (b) vortices excited Raman spectra, and (c) topological charge-dependent Raman modes shifts of chiral SWNTs.

shown in Fig. 3. This means the optical vortex can also tailor the absorption of chiral SWNTs, giving rise to a tunable Raman response. Moreover, worth noting is that the intensities of Raman modes of these three SWNTs are all attenuated when the topological charge is increased. This can be also interpreted as a consequence of the decreased optical absorption: with the increasing of topological charge, the amount of absorbed photon is reduced, leading to the reduction of phonon number emitted during the Raman process.

In conclusion, we have proposed a strategy for controlling the Raman response of SWNTs by utilizing the OAM of the optical vortex. Obvious blueshifts of Raman modes are observed as the OAM content of excitation is increased. We analyzed Raman shifts of SWNTs by using the full-wave simulation. It is revealed that the optical absorption of the SWNT deceases with the increasing of the OAM content. This absorption drop suppresses the softening of C–C bonds, and is responsible for the blueshifts of Raman modes. Our work provides an active and flexible way to control the spectra response of the SWNT and facilitates the understanding of the OAM modulated light matter interactions in single molecular level.

Funding. National Natural Science Foundation of China (NSFC) (11634010, 61675170, 61308031, 51522201, 11474006, 61377035); Fundamental Research Funds for the Central Universities (3102015ZY062); Natural Science Foundation of Shanghai (17ZR1414300).

REFERENCES

1. M. Freitag, Y. Martin, J. A. Misewich, R. Martel, and P. H. Avouris, Nano Lett. **3**, 1067 (2003).
2. L. Yang, S. Wang, Q. Zeng, Z. Zhang, T. Pei, Y. Li, and L. Peng, Nat. Photonics **5**, 672 (2011).
3. R. Miura, S. Imamura, R. Ohta, A. Ishii, X. Liu, T. Shimada, S. Iwamoto, Y. Arakawa, and Y. K. Kato, Nat. Commun. **5**, 5580 (2014).
4. D. Y. Joh, J. Kinder, L. H. Herman, S. Y. Ju, M. A. Segal, J. N. Johnson, G. K. L. Chan, and J. Park, Nat. Nanotechnol. **6**, 51 (2011).
5. A. E. Nikolaenko, F. De Angelis, S. A. Boden, N. Papasimakis, P. Ashburn, E. Di Fabrizio, and N. I. Zheludev, Phys. Rev. Lett. **104**, 153902 (2010).
6. N. Rauhut, M. Engel, M. Steiner, R. Krupke, P. Avouris, and A. Hartschuh, ACS Nano **6**, 6416 (2012).
7. M. Takase, H. Ajiki, Y. Mizumoto, K. Komeda, M. Nara, H. Nabika, S. Yasuda, H. Ishihara, and K. Murakoshi, Nat. Photonics **7**, 550 (2013).
8. N. Mauser, N. Hartmann, M. S. Hofmann, J. Janik, A. Hogele, and A. Hartschuh, Nano Lett. **14**, 3773 (2014).
9. R. Watahiki, T. Shimada, P. Zhao, S. Chiashi, S. Iwamoto, Y. Arakawa, S. Maruyama, and Y. Kato, Appl. Phys. Lett. **101**, 141124 (2012).
10. X. D. Ma, O. Roslyak, F. Wang, J. G. Duque, A. Piryatinski, S. K. Doorn, and H. Htoon, ACS Nano **8**, 10613 (2014).
11. E. Gaufres, N. Izard, X. Le Roux, D. Marris-Morini, S. Kazaoui, E. Cassan, and L. Vivien, Appl. Phys. Lett. **96**, 231105 (2010).
12. G. Volpe, G. Molina-Terriza, and R. Quidant, Phys. Rev. Lett. **105**, 216802 (2010).
13. M. Aeschlimann, M. Bauer, D. Bayer, T. Brixner, S. Cunovic, F. Dimler, A. Fischer, W. Pfeiffer, M. Rohmer, C. Schneider, F. Steeb, C. Struber, and D. V. Voronine, Proc. Natl. Acad. Sci. USA **107**, 5329 (2010).
14. S. Kosmeier, A. C. De Luca, S. Zolotovskaya, A. Di Falco, K. Dholakia, and M. Mazilu, Sci. Rep. **3**, 1808 (2013).
15. M. Babiker, C. R. Bennett, D. L. Andrews, and L. C. D. Romero, Phys. Rev. Lett. **89**, 143601 (2002).
16. A. Alexandrescu, D. Cojoc, and E. Di Fabrizio, Phys. Rev. Lett. **96**, 243001 (2006).
17. H. Seidel, L. Csepregi, A. Heuberger, and H. Baumgartel, J. Electrochem. Soc. **137**, 3612 (1990).
18. S. M. Huang, X. Y. Cai, and J. Liu, J. Am. Chem. Soc. **125**, 5636 (2003).
19. X. S. Wang, Q. Q. Li, J. Xie, Z. Jin, J. Y. Wang, Y. Li, K. L. Jiang, and S. S. Fan, Nano Lett. **9**, 3137 (2009).
20. K. H. Liu, Z. Xu, W. L. Wang, P. Gao, W. Y. Fu, X. D. Bai, and E. G. Wang, J. Phys. D **42**, 125412 (2009).
21. C. Maurer, A. Jesacher, S. Bernet, and M. Ritsch-Marte, Laser Photon. Rev. **5**, 81 (2011).
22. K. H. Liu, W. L. Wang, M. H. Wu, F. J. Xiao, X. P. Hong, S. Aloni, X. D. Bai, E. G. Wang, and F. Wang, Phys. Rev. B **83**, 113404 (2011).
23. M. S. Dresselhaus, G. Dresselhaus, A. Jorio, A. G. Souza, and R. Saito, Carbon **40**, 2043 (2002).
24. M. Y. Sfeir, F. Wang, L. M. Huang, C. C. Chuang, J. Hone, S. P. O'Brien, T. F. Heinz, and L. E. Brus, Science **306**, 1540 (2004).
25. A. Bassil, P. Puech, L. Tubery, W. Bacsa, and E. Flahaut, Appl. Phys. Lett. **88**, 173113 (2006).
26. Y. Y. Zhang, H. Son, J. Zhang, J. Kong, and Z. F. Liu, J. Phys. Chem. C **111**, 1988 (2007).
27. M. Zdrojek, J. Judek, and M. Wasik, Phys. Rev. Lett. **108**, 225501 (2012).
28. N. R. Raravikar, P. Keblinski, A. M. Rao, M. S. Dresselhaus, L. S. Schadler, and P. M. Ajayan, Phys. Rev. B **66**, 235424 (2002).
29. L. J. Ci, Z. P. Zhou, L. Song, X. Q. Yan, D. F. Liu, H. J. Yuan, Y. Gao, J. X. Wang, L. F. Liu, W. Y. Zhou, G. Wang, and S. S. Xie, Appl. Phys. Lett. **82**, 3098 (2003).
30. R. Saito, M. Fujita, G. Dresselhaus, and M. S. Dresselhaus, Phys. Rev. B **46**, 1804 (1992).
31. M. F. Lin and K. W. K. Shung, Phys. Rev. B **52**, 8423 (1995).
32. G. Y. Slepyan, S. A. Maksimenko, A. Lakhtakia, O. Yevtushenko, and A. V. Gusakov, Phys. Rev. B **60**, 17136 (1999).
33. K. H. Liu, J. Deslippe, F. J. Xiao, R. B. Capaz, X. P. Hong, S. Aloni, A. Zettl, W. L. Wang, X. D. Bai, S. G. Louie, E. G. Wang, and F. Wang, Nat. Nanotechnol. **7**, 325 (2012).
34. G. Y. Slepyan, M. V. Shuba, S. A. Maksimenko, and A. Lakhtakia, Phys. Rev. B **73**, 195416 (2006).
35. A. S. Rury and R. Freeling, Phys. Rev. A **86**, 053830 (2012).
36. G. Guzzinati, A. Béché, H. Lourenço-Martins, J. Martin, M. Kociak, and J. Verbeeck, Nat. Commun. **8**, 14999 (2017).